Development 140, 3595-3600 (2013) doi:10.1242/dev.091033

Cranial neural crest cells form corridors prefiguring sensory neuroblast migration

Sabine Freter[1], Stephen J. Fleenor[1], Rasmus Freter[2], Karen J. Liu[3] and Jo Begbie[1,*]

SUMMARY

The majority of cranial sensory neurons originate in placodes in the surface ectoderm, migrating to form ganglia that connect to the central nervous system (CNS). Interactions between inward-migrating sensory neuroblasts and emigrant cranial neural crest cells (NCCs) play a role in coordinating this process, but how the relationship between these two cell populations is established is not clear. Here, we demonstrate that NCCs generate corridors delineating the path of migratory neuroblasts between the placode and CNS in both chick and mouse. *In vitro* analysis shows that NCCs are not essential for neuroblast migration, yet act as a superior substrate to mesoderm, suggesting provision of a corridor through a less-permissive mesodermal territory. Early organisation of NCC corridors occurs prior to sensory neurogenesis and can be recapitulated *in vitro*; however, NCC extension to the placode requires placodal neurogenesis, demonstrating reciprocal interactions. Together, our data indicate that NCC corridors impose physical organisation for precise ganglion formation and connection to the CNS, providing a local environment to enclose migrating neuroblasts and axonal processes as they migrate through a non-neural territory.

KEY WORDS: Neural crest, Placode, Cranial sensory ganglia

INTRODUCTION

Sensory ganglia in the head and trunk are generated from migratory populations of cells. In the trunk, they develop from neural crest cells (NCC) that migrate into the rostral somite. A subpopulation of these NCCs stop lateral to the neural tube and coalesce, before undergoing neurogenesis to form the dorsal root ganglia (DRG) (George et al., 2010). The imposition of this migration pattern by the somites leads to the regular, segmental organisation of the DRG and their innervation of the central nervous system (CNS) (Gammill and Roffers-Agarwal, 2010).

The cranial sensory ganglia (CSG) are more complex in organisation and embryonic origin. The CSG can be subdivided into proximal and distal ganglia relating to location on the associated cranial nerve. Neurons of the proximal CSG are generated from NCCs (D'Amico-Martel and Noden, 1983; Thompson et al., 2010). However, in the distal CSG, NCCs mainly generate the non-neuronal components, whereas the majority of neurons originate in ectodermal neurogenic placodes (D'Amico-Martel and Noden, 1983; Harlow et al., 2011; Thompson et al., 2010). With the exception of the ophthalmic trigeminal placode, which generates postmitotic neurons, neurogenic placodes produce neuroblasts that delaminate and actively migrate towards the hindbrain (Begbie et al., 2002; Blentic et al., 2011; Graham et al., 2007; McCabe et al., 2009). In the head, unlike the trunk, there is no architectural framework to guide CSG formation; so how is neuroblast migration controlled to pattern the CSG and their accurate innervation of the hindbrain?

Reports across a range of species demonstrate that NCCs play a role in organising the CSG. Our studies in chick show that loss of cranial NCCs either by physical ablation or by ectopic neuropilin expression, affects accurate CSG formation (Begbie and Graham, 2001; Osborne et al., 2005). Similarly, zebrafish mutants lacking a subpopulation of NCCs show defective ganglion formation (Culbertson et al., 2011). Complementary studies in mice show that ectopic NCC migration is associated with ectopic cranial sensory neuron migration (Chen et al., 2011; Schwarz et al., 2008). Analysis of the molecular interactions between the two populations has mainly been carried out in the developing trigeminal ganglion, and shows roles for Robo and Wnt signalling pathways (Shiau and Bronner-Fraser, 2009; Shiau et al., 2008; Shigetani et al., 2008). Here, we examine the cellular relationship between the NCCs and placodal neuroblasts underlying the organisation of the CSG, and address how NCCs are positioned to play this role.

MATERIALS AND METHODS

Animals

Fertilised hens' eggs (Winter Egg Farm, UK) were incubated in a humidified chamber at 38°C to the required Hamburger Hamilton stage (Hamburger and Hamilton, 1992). The mouse line used was Wnt1cre:R26RYFP (Danielian et al., 1998; Srinivas et al., 2001). Embryos from both species were fixed overnight at 4°C in 1×MEMFA, washed with 1×PBS, stored in 1×PBS+0.02% azide before antibody staining. Mouse work was approved by the King's College London Ethical Review Process and was performed in accordance with UK Home Office Project Licence 70/7441 (K.J.L.).

Antibody staining and *in situ* hybridisation

Whole-mount antibody staining was carried out as described previously (Thompson et al., 2010). Primary antibodies were: mouse anti-HNK1, 1:200 (Sigma); mouse anti-neurofilament medium chain, 1:5000 (RMO-270, Zymed, Invitrogen); mouse anti-islet 1/2, 1:1000 (a kind gift from Ivo Lieberam, King's College London, UK); rabbit anti-GFP, 1:500 (Invitrogen). Secondary antibodies were: Alexa 488-conjugated anti-mouse IgG; Alexa 488-conjugated anti-rabbit IgG; Alexa 568-conjugated anti-

[1]Department of Physiology, Anatomy and Genetics, University of Oxford, South Parks Road, Oxford OX1 3QX, UK. [2]Ludwig Institute for Cancer Research, Nuffield Department of Clinical Medicine, University of Oxford, Oxford OX3 7DQ, UK. [3]Department of Craniofacial Development, King's College London, London SE1 9RT, UK.

*Author for correspondence (jo.begbie@dpag.ox.ac.uk)

Accepted 20 June 2013

mouse IgM; Alexa 647-conjugated anti-mouse IgM used at 1:1000 (Invitrogen Molecular Probes).

Single and double whole-mount *in situ* hybridisation was carried out as described previously (Begbie et al., 1999). For triple labelling, whole-mount *in situ* hybridisation was carried out using the FastRed substrate (Sigma), and then whole-mount antibody staining carried out as above. The FastRed signal was visualised at 568 nm and Alexa-conjugated antibodies at 488 nm and 647 nm by confocal.

Cell labelling

In ovo electroporation was used to introduce chick β-actin GFP (2 μg/μl) into presumptive placodal ectoderm at HH15 using 4×5 msecond 10 V pulses, or hindbrain crest at HH9 using 5×5 msecond 10 V pulses (Graham et al., 2007).

In vitro culture

Placodes

For neural crest cultures, midbrain and hindbrain segments from HH9 (6-9 somites) embryos were cultured for 24 hours to allow NCCs to establish, then neural tubes were removed. Lateral plate mesoderm caudal to the last somite was taken from the same embryos and cultured for 24 hours prior to addition of placode. Placodes were taken at HH17 from GFP electroporated embryos targeted at HH14 using flame-sharpened tungsten needles. Placodes were plated on top of neural crest, mesoderm or FN, in F12+N2, allowed to settle for 15 minutes then cultured for 24 hours at 37°C in 5% CO_2.

Neural tube

Neural tubes from diencephalon to first somite level were excised from HH9 (6-9 somite) embryos using tungsten needles. Neural tubes were carefully positioned on fibronectin-coated coverslips (10 μg/ml) and cultured for 22 hours in F12+N2 at 37°C in 5% CO_2.

Targeted ablation of placodal neurons

The diphtheria toxin α-chain expression vector (CMV-TdTomato-2A-DtA) was produced as follows. The expression vector pCMV-tdT-2A-MCS was derived from peCFP-N1 (Clontech) by replacing the eCFP-coding region with tdTomato excised from pCS2-tdTomato-2A-GFP (a kind gift from Shankar Srinivas, University of Oxford, UK) with Nhe(Xba)/*Bsr*G1. A synthetic 2A peptide sequence followed by a multiple cloning site inserted using *Bsr*G1/*Not*I. Co-translational cleavage of the 2A sequence was validated to exceed 0.95 with various inserts. DTA from pR26-IRES-eGFP was cloned into backbone pCMV-tdT-2A-MCS using *Bam*H1 and *Not*I. All cloning products were confirmed by sequencing.

In ovo electroporation was used to introduce CMV-TdTomato-2A-DtA (4 μg/μl) unilaterally into placodal ectoderm at HH13-14 as above and embryos incubated to HH16-18.

Embryo visualisation

Embryos after whole-mount *in situ* hybridisation were imaged using a Zeiss Stereolumar stereomicroscope. Confocal analysis of whole embryos was performed at ×10 and ×20 magnification acquiring optical sections at 2 μm intervals (Zeiss LSM710). For 75 μm transverse vibratome sections, embryos were embedded in 15% gelatin:15% sucrose:PBS and fixed overnight (MEMFA). Confocal analysis of sections was performed at ×20 and ×40 magnification, acquiring optical sections at 1 μm intervals (Zeiss LSM710). Volocity visualisation software (Perkin-Elmer) was used for 3D reconstruction.

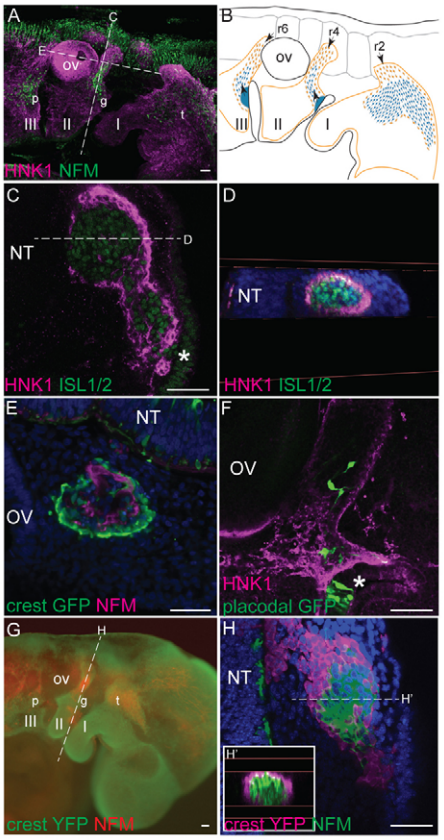

Fig. 1. Neural crest cells form corridors associated with sensory neuroblasts in chick and mouse. (**A**,**B**) Lateral view of HH15$^+$ chick embryo showing association of NCCs with neuroblasts in (A) a 3D reconstruction of HNK1 (magenta) and NFM (green) staining, and (B) a schematic representation (NCCs, orange; neuroblasts, blue; general NCC territory is shown by an orange line; the direction of migration is indicated by arrows). (**C**,**D**) HH17 transverse section (C) and digital coronal re-section (D) reveal HNK1$^+$ NCCs (magenta) peripheral to ISL$^+$ neuroblasts (green) (single optical confocal section). (**E**) NCC labelling by GFP electroporation confirms NCCs (green) encircle NFM$^+$ neuroblasts (magenta); HH18 coronal section. (**F**) Following placode electroporation, bipolar GFP$^+$ cells (green) are seen migrating within the HNK1$^+$ NCC corridor (magenta) (sagittal, HH17, single optical confocal section). (**G**) Lateral view of 29 ss Wnt1cre:R26RYFP mouse embryo shows the association of NCCs (green) with NFM$^+$ neuroblasts (red). (**H**,**H′**) Transverse section (H) and digital coronal re-section (H′) show YFP$^+$ NCCs (magenta) encircling NFM$^+$ neuroblasts (green) as in chick (confocal stack projection). Asterisks indicate placodes; I, II and III, pharyngeal arches 1, 2 and 3; NT, neural tube; OV, otic vesicle; p, petrosal; g, geniculate; t, trigeminal ganglia; r, rhombomere. Dotted lines in A indicate the levels of sections in C,E; dotted lines in C indicate the level of the section in D; dotted lines in G indicate the level of the section in H; dotted lines in H indicate the level of the section in H′. Scale bar: 100 μm.

RESULTS AND DISCUSSION

Cranial neural crest cells assemble into corridors delineating sensory ganglion formation

Three-dimensional reconstruction of HNK1- (glycan epitope labelling NCC) and NFM- (neurofilament medium chain; neuroblasts) stained chick embryos revealed that early hindbrain NCC streams were maintained, forming robust structures between hindbrain and pharyngeal arches (Fig. 1A,B; supplementary material Movie 1). These NCC structures were associated with the migrating neuroblasts (Fig. 1A,B), with HNK1 staining localised peripherally to the neuroblast population in all of the CSG examined (Fig. 1A,C,D). This tube-like appearance suggests that NCCs form a corridor delineating the path of the neuroblasts from their birthplace in the placodal epithelium towards the hindbrain. To confirm the NCC origin of these structures, we labelled pre-migratory NCCs by in ovo GFP electroporation. As predicted, the GFP$^+$ NCC encircled the migrating neuroblasts (Fig. 1E).

To address neuroblast behaviour within the HNK1$^+$ NCC corridor, we visualised individual GFP-labelled neuroblasts in whole embryos (Fig. 1F; supplementary material Movies 2, 3). In all embryos analysed (n=4), the neuroblasts were located deep within the corridor, and neither the GFP$^+$ cell bodies nor their processes crossed the HNK1$^+$ NCCs. This suggests that the HNK1$^+$ NCCs provide a physical barrier constraining neuroblast migration. Three-dimensional reconstruction showed that at stages of peak neuroblast migration, HNK1$^+$ NCCs extended directly to the edges of the placode (asterisk in Fig. 1F), enclosing the neuroblasts as they delaminate from the epithelium (supplementary material Movie 3). We propose that the NCCs form a physical corridor through a non-neural territory, funnelling the neuroblasts inwards as they exit from the surface ectoderm.

Neural crest corridors are conserved in chick and mouse

To determine whether the NCC corridor is also present in mice, we used the Wnt1cre:R26RYFP mouse line, genetically labelling NCCs (Danielian et al., 1998; Srinivas et al., 2001). As in the chick, YFP$^+$ NCCs formed a structure extending between the hindbrain and the top of the pharyngeal arches (Fig. 1G). Confocal analysis showed YFP$^+$ NCCs encircling the NFM$^+$ neuroblasts (Fig. 1H,H′). Studies in mice show that mutations affecting NCC patterning are reflected by defects in CSG patterning, but that genetic NCC ablation has less effect (Chen et al., 2011; Coppola et al., 2010; Golding et al., 2000; Schwarz et al., 2008). We suggest that the NCC corridor provides a physical constraint for neuroblasts with an inherent ability to migrate, rather than an active guidance mechanism. As such, neuroblasts would still migrate in the absence of NCC, albeit less accurately, whereas a NCC patterning defect causing a misplaced corridor would have more effect on CSG patterning.

In vitro behaviour of placodal neuroblasts on NCC versus mesoderm

Our hypothesis favours physical constraint versus active guidance by NCCs. We tested this by comparing neuroblast behaviour from isolated placodes cultured on NCCs with those cultured on fibronectin (FN) alone, or on lateral plate mesoderm. Explants cultured on NCC showed cells exiting together and extending long processes with small growth cones (n=6) (Fig. 2A; growth cone, arrowhead in 2A′ and ×40 inset). These explants were similar to explants cultured on FN alone (n=4) (Fig. 2B), suggesting that NCCs do not provide active guidance to the neuroblasts. By comparison, mesoderm provided a less favourable substrate for migration. In these explants the neuroblast processes were less straight and shorter with fewer projections exiting from the ×10 field (Fig. 2C,D) and larger growth cones (n=4) (arrowhead, Fig. 2C′ and ×40 inset). This reinforces the idea that the NCC corridor provides a physical setting for inherent neuroblast migration and axon extension through a less-permissive mesodermal environment between placode and neural tube.

Neural crest corridor development

We used *Isl1* and *Sox10* double *in situ* hybridisation to examine how these NCC structures assemble with respect to epibranchial placode neuroblast production. At HH13 there is a clear dorsal Sox10$^+$ stream (arrowheads in Fig. 3A,A′), but this does not extend to the first neuroblasts of the geniculate placode (asterisk in Fig. 3A,A′). As neurogenesis becomes established, the Sox10$^+$ NCC corridor extends towards the placodes (Fig. 3B,B′)

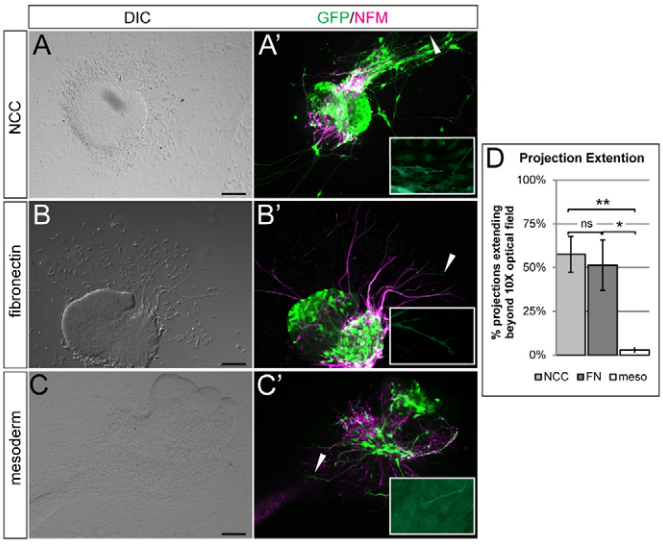

Fig. 2. *In vitro* behaviour of placodal neuroblasts. (**A-C′**) In GFP-electroporated (green), NFM-labelled (magenta) placode cultures on NCCs (A), neuroblasts exit together, extending long processes with small growth cones (A′, arrowhead; inset is at 4× higher magnification than the main panel). Morphology is similar to placodes on FN (B; growth cone indicated by arrowhead in B′; inset is at 4× higher magnification than the main panel), but distinct from placodes on lateral plate mesoderm, where exiting neuroblasts have shorter processes with large growth cones (C; growth cone indicated by arrowhead in C′; inset is at 4× higher magnification than the main panel). (**D**) The percentage of projections extending beyond the ×10 optical field. NCC, 57.56±10.18%; FN, 51.37±14.51%; meso, 2.79±1.61%. Error bars indicate s.e.m. Statistical analysis using Student's t-test, $^{**}P$=0.0027; $^{*}P$=0.0432; not significant, P=0.7393. Scale bar: 100 μm.

and by HH17 there is a clear extension of Sox10$^+$ NCCs surrounding the neuroblasts delaminating from the placode (Fig. 3C,C′).

We compared this with HNK1$^+$ NCC corridor development, combining *Sox10* staining with HNK1 and ISL1 antibody labelling. HNK1 is a carbohydrate epitope added to many different glycolipids and glycoproteins that has been shown to recognise NCC (Tucker et al., 1984), whereas *Sox10* is one of the earliest NCC-specifying genes that later is maintained and required for non-ectomesenchymal lineages (Sauka-Spengler and Bronner-Fraser, 2008). At HH13, most NCC were *Sox10*/HNK1 double positive (white in Fig. 3E). By HH14$^+$, HNK1 staining (magenta) was restricted to the mesodermal interface, encircling a core of *Sox10*$^+$ NCCs (yellow) (Fig. 3F). At the peak of placodal neuroblast migration (HH17), the HNK1 staining (magenta) formed a sheath around the *Sox10*$^+$ NCCs (yellow), which in turn surrounded the ISL$^+$ neuroblasts (Fig. 3D,G). The peripheral localisation of HNK1 staining compared with Sox10$^+$ NCCs, and the extension to the placode are clear in 3D embryo reconstruction (see supplementary material Movie 3; Fig. 1F; Fig. 3J).

We examined HNK1 staining in GFP$^+$ NCC-labelled chick embryos at HH14, prior to CSG formation. Coronal sections showed that HNK1 specifically labelled GFP$^+$ cells at the interface with the mesoderm (white arrowhead, Fig. 3H). This is before significant peripheral neurogenesis, suggesting that the neuroblasts do not play a crucial role in initial establishment of the NCC corridors. Interestingly, YFP$^+$ NCC corridors were also seen in mouse embryos with few neuroblasts (E9, Fig. 3I).

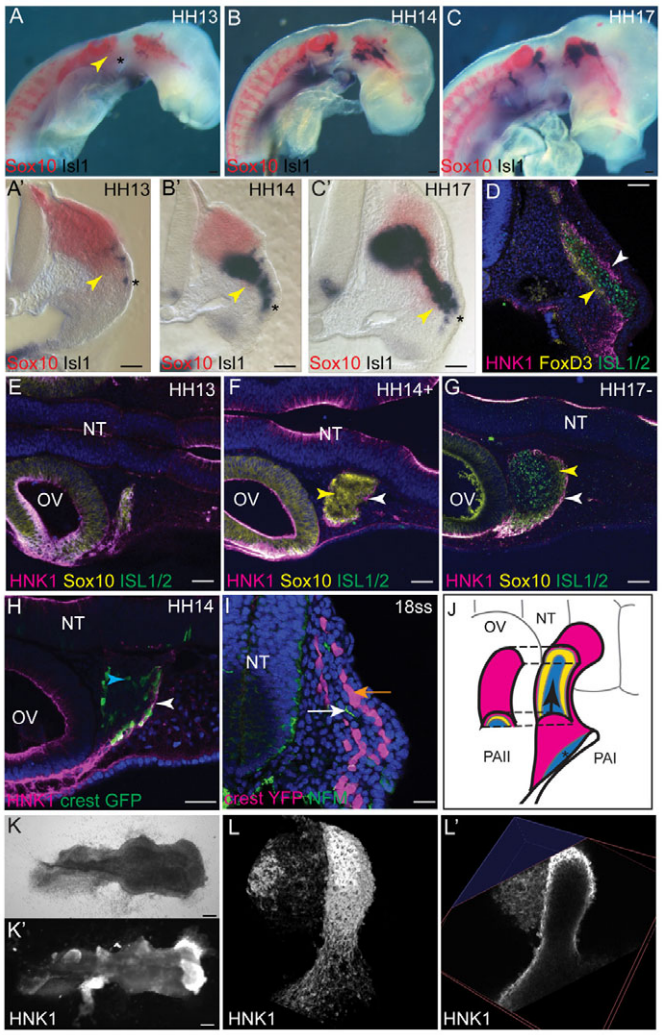

Fig. 3. Neural crest corridor development. (**A-C**) Lateral view of *Sox10/Isl1* double-labelled chick embryos showing NCC corridor development in relation to developing CSG. (**A′-C′**) Transverse sections reveal extension of Sox10$^+$ NCCs (yellow arrowheads indicate ventral point) to placode (asterisks) with increasing neurogenesis. (**D**) Transverse section of triple-labelled HH17 chick (D) shows HNK1$^+$ NCCs (magenta; white arrowhead) and *Foxd3*$^+$ NCCs (yellow; yellow arrowhead), surrounding ISL$^+$ neuroblasts (green) (confocal stack projection). (**E-G**) Coronal sections show restriction of HNK1 staining to periphery of NCC corridor (confocal stack projection). At HH13, NCCs are Sox10/HNK1 double positive (E), but by HH14$^+$ (F) HNK1 staining (magenta; white arrowhead) is localised to the periphery of Sox10$^+$ NCCs (yellow; yellow arrowhead). At HH17–, ISL1$^+$ neuroblasts can be seen at core of NCC corridor (G). (**H**) Coronal section of GFP NCC electroporated chick confirms restriction of HNK1 staining (magenta; white arrowhead) to periphery of total GFP$^+$ NCCs (green; blue arrowhead) at HH14 prior to robust neurogenesis (single optical confocal section). (**I**) Analysis in mouse at 18 ss also shows YFP$^+$ NCCs (magenta; orange arrow) forming corridors containing few NFM$^+$ processes (green; white arrow). (**J**) Schematic representation of the NCC corridor with HNK1$^+$ NCCs (magenta) surrounding Sox10$^+$ NCCs (yellow), extending to the placode (asterisk). Neuroblasts (blue) migrate at the NCC corridor centre. Arrow indicates direction of migration. (**K**,**K′**) Chick hindbrain explants demonstrate *in vitro* streamed NCC migration with DIC (K) and HNK1 (K′). (**L**,**L′**) Confocal analysis reveals 3D nature of *in vitro* HNK1$^+$ NCC corridor (L), whereas digital re-section reveals peripheral HNK1 staining (L′). Asterisks indicate placode; NT, neural tube; OV, otic vesicle; PAI, PAII, pharyngeal arches I and II. Scale bar: 100 μm.

Together, these data suggest that the initial establishment of NCC corridors adjacent to the neural tube occurs in the absence of placodal neurogenesis, but that the extension to the placode requires the production of neurons.

Neural crest cells organise into corridors *in vitro*

Previous work in the axolotl has shown that cranial NCCs will form streams *in vitro* (Cerny et al., 2004). To test whether chick NCCs could form streams and associated HNK$^+$ corridors *in vitro*, we cultured HH9 cranial neural tubes (hindbrain to diencephalon) upright on fibronectin (FN). After 22 hours, distinct HNK1$^+$ staining was seen at discrete intervals along the hindbrain explant (12/12). In a small number of cases (3/12), HNK1$^+$ NCC formed distinct streams directly on the FN which showed little three-dimensionality. However, in 9/12 cases, 3D HNK1$^+$ NCC structures were seen extending from the dorsal hindbrain down to the FN (Fig. 3K,K′). Confocal analysis of these samples showed that the HNK1$^+$ staining was restricted to the periphery (Fig. 3L,L′). This demonstrates that organisation into 3D structures with peripheral HNK1 staining is intrinsic to the NCCs.

Interactions between the neural crest cells and placodal neuroblasts are required for correct NCC corridor formation

Our expression analysis suggested that the extension of the NCC corridor to the placode requires the presence of placodal neuroblasts. To test this, the diphtheria toxin α-chain (DTA) was electroporated into ectoderm to eliminate the placode with minimal mechanical disruption. *Isl1* and *Phox2b* staining showed a severe reduction in neurons in the DTA-targeted region compared with the contralateral side: *Isl1* (15/17; 88%: Fig. 4A) and *Phox2b* (5/6; 83%: Fig. 4B). *Sox10* staining showed that the NCC corridor did not form correctly on the DTA-targeted side, losing the extension to the placode (17/22; 77%: Fig. 4C). *Isl1* and *Sox10* double labelling showed a clear correlation between neuroblast ablation and the failure of Sox10$^+$ NCCs to reach the placode (25/38; 66%: Fig. 4D). Although analysis was mainly carried out at rhombomere 4 (r4) (Fig. 4), the effect was also seen at r6 (supplementary material Fig. S1). Control GFP-electroporated embryos were normal for all markers analysed (*n*=*Isl*: 10; *Phox2b*: 5; *Sox10*: 11; double *Isl1*/*Sox10*: 5). Earlier *Isl1*/*Sox10* analysis was carried out to determine whether Sox10$^+$ NCCs reached the placode before being lost, and showed that the Sox10$^+$ NCCs were still absent beneath the ectoderm (DTA, *n*=3/3; GFP, *n*=2/2; Fig. 4E). Furthermore, analysis of apoptosis using lysotracker showed cell death in NCCs, but no observable increase following placode ablation compared with contralateral side (DTA, *n*=12; Fig. 4F), or control electroporation (GFP, *n*=11; data not shown).

Our data show that although the NCC corridor is required to facilitate the correct neuroblast migration and axon projection inwards, the neuroblasts themselves are necessary for the correct formation of the NCC corridor. We suggest that the extension to the placode occurs by migration of Sox10$^+$ NCCs; however, our results cannot confirm this. Interestingly, in *Drosophila*, peripheral glia form tubes required for accurate sensory axon entry to the CNS, and studies have described similar reciprocal interactions between the two cell types (Sepp and Auld, 2003; Sepp et al., 2001).

Conclusions

Our results demonstrate that cranial NCC streams transform into corridors that are subsequently associated with migrating sensory neuroblasts in chick and mouse. We propose that the NCC corridor

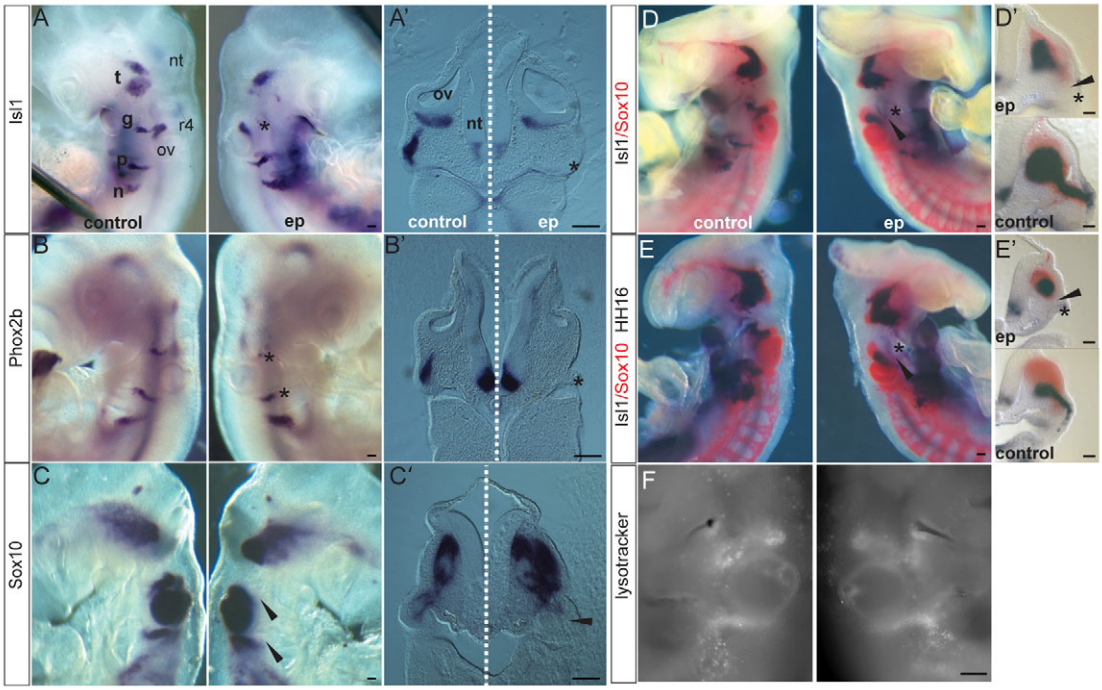

Fig. 4. Placode ablation affects neural crest corridor formation. (**A-C′**) Sections at r4 level of DTA-electroporated chick embryos at HH18. *Isl1* (88%; *n*=17) (A,A′) and *Phox2b* (83%; *n*=6) (B,B′) both demonstrate reduction in neuroblasts migrating from targeted placodes (asterisks) on electroporated side (ep) compared with unelectroporated side (control). (C,C′) *Sox10* reveals failure of NCC corridor extension (arrowheads) to targeted placodes (77%; *n*=22). (**D**,**D′**) *Sox10/Isl1* confirms reduction in NCC corridor (arrowhead) correlates with loss of neuroblasts (asterisks) (66%; *n*=38), seen clearly in transverse sections comparing DTA (ep) with GFP (control). (**E**,**E′**) Earlier *Sox10/Isl1* staining (HH16) still demonstrates Sox10^{+} NCC deficiency at the targeted placode; compare DTA (ep) with GFP (control). (**F**) Lysotracker staining for apoptosis shows no significant increase in NCC cell death in ep compared with control. nt, neural tube; ov, otic vesicle; g, n, p, t, geniculate, nodose, petrosal and trigeminal ganglia; r, rhombomere. Scale bar: 100 μm.

provides structural organisation for the CSG, bridging the mesodermal domain between the placodal epithelium and the CNS, for the inward migration of neuroblasts and their axonal extensions (Fig. 3J). In chick, an anatomical structure funnelling cells in from the surface ectoderm was first suggested as long ago as 1893 (Goronowitsch, 1893), and an HNK1 scaffold associated with developing cranial nerves in 1991 (Layer and Kaulich, 1991). Here, we have confirmed that NCCs generate a structural corridor and have shown that it is present in mice. Within the CNS, physical corridors for neuronal migration and axon guidance have been described in the form of astrocytic tubes promoting neuroblast migration in the rostral migratory stream and tangentially migrating corridor cells guiding thalamocortical axons in the telencephalon (Lois et al., 1996; López-Bendito et al., 2006). Interestingly, however, although these structures facilitate migration within the CNS, the NCC corridor described here traverses a non-neural territory.

The use of corridors for neuronal migration in peripheral nervous system (PNS) development has not been described before. It is possible that, in the trunk, NCC corridors also provide a physical cue for control of migration and axon guidance. However, as trunk sensory neurons themselves are derived from NCCs this is difficult to determine. In support of the hypothesis, we can turn to studies of axon regeneration in the adult trunk after injury. These show that endoneurial tubes constrain axon growth following nerve crush (Nguyen et al., 2002), whereas following transection Schwann cells dedifferentiate and form bridges that act as guides for regenerating axons (Parrinello et al., 2010). Furthermore, recent studies have shown that olfactory ensheathing cells, which enhance the correct re-establishment of axonal connections, are also derived from neural crest cells (Barraud et al., 2010). The cranial NCC corridors are neural crest cells as opposed to Schwann cells, but suggest an exciting developmental parallel to the regeneration scenario.

Acknowledgements
We thank Ivo Lieberam for Isl1/2 antibody, Alexandra Smith for electroporations for explants, and Britta Eickholt, Anthony Graham, Raj Ladher and Clive Wilson for comments on the manuscript.

Funding
Supported by the Biotechnology and Biological Sciences Research Council [BB/G011524/1 to J.B.; BB/I021922/1 to K.J.L.]; Oxford University Press John Fell Fund to J.B.; and the Wellcome Trust [studentship 092920/Z/10/Z to S.J.F.; WT081880AIA to K.J.L.]. Deposited in PMC for immediate release.

Competing interests statement
The authors declare no competing financial interests.

Author contributions
Experiments and analysis were carried out by S.F., S.J.F. and J.B.; the DTA construct was designed and generated by R.F.; mouse embryos were provided by K.J.L.; experimental design and manuscript preparation were by J.B.

Supplementary material
Supplementary material available online at
http://dev.biologists.org/lookup/suppl/doi:10.1242/dev.091033/-/DC1

References

Barraud, P., Seferiadis, A. A., Tyson, L. D., Zwart, M. F., Szabo-Rogers, H. L., Ruhrberg, C., Liu, K. J. and Baker, C. V. (2010). Neural crest origin of olfactory ensheathing glia. *Proc. Natl. Acad. Sci. USA* **107**, 21040-21045.
Begbie, J. and Graham, A. (2001). Integration between the epibranchial placodes and the hindbrain. *Science* **294**, 595-598.
Begbie, J., Brunet, J. F., Rubenstein, J. L. and Graham, A. (1999). Induction of the epibranchial placodes. *Development* **126**, 895-902.

Begbie, J., Ballivet, M. and Graham, A. (2002). Early steps in the production of sensory neurons by the neurogenic placodes. *Mol. Cell. Neurosci.* **21**, 502-511.
Blentic, A., Chambers, D., Skinner, A., Begbie, J. and Graham, A. (2011). The formation of the cranial ganglia by placodally-derived sensory neuronal precursors. *Mol. Cell. Neurosci.* **46**, 452-459.
Cerny, R., Meulemans, D., Berger, J., Wilsch-Bräuninger, M., Kurth, T., Bronner-Fraser, M. and Epperlein, H. H. (2004). Combined intrinsic and extrinsic influences pattern cranial neural crest migration and pharyngeal arch morphogenesis in axolotl. *Dev. Biol.* **266**, 252-269.
Chen, Y., Takano-Maruyama, M. and Gaufo, G. O. (2011). Plasticity of neural crest-placode interaction in the developing visceral nervous system. *Dev. Dyn.* **240**, 1880-1888.
Coppola, E., Rallu, M., Richard, J., Dufour, S., Riethmacher, D., Guillemot, F., Goridis, C. and Brunet, J. F. (2010). Epibranchial ganglia orchestrate the development of the cranial neurogenic crest. *Proc. Natl. Acad. Sci. USA* **107**, 2066-2071.
Culbertson, M. D., Lewis, Z. R. and Nechiporuk, A. V. (2011). Chondrogenic and gliogenic subpopulations of neural crest play distinct roles during the assembly of epibranchial ganglia. *PLoS ONE* **6**, e24443.
D'Amico-Martel, A. and Noden, D. M. (1983). Contributions of placodal and neural crest cells to avian cranial peripheral ganglia. *Am. J. Anat.* **166**, 445-468.
Danielian, P. S., Muccino, D., Rowitch, D. H., Michael, S. K. and McMahon, A. P. (1998). Modification of gene activity in mouse embryos in utero by a tamoxifen-inducible form of Cre recombinase. *Curr. Biol.* **8**, 1323-1326.
Gammill, L. S. and Roffers-Agarwal, J. (2010). Division of labor during trunk neural crest development. *Dev. Biol.* **344**, 555-565.
George, L., Kasemeier-Kulesa, J., Nelson, B. R., Koyano-Nakagawa, N. and Lefcort, F. (2010). Patterned assembly and neurogenesis in the chick dorsal root ganglion. *J. Comp. Neurol.* **518**, 405-422.
Golding, J. P., Trainor, P., Krumlauf, R. and Gassmann, M. (2000). Defects in pathfinding by cranial neural crest cells in mice lacking the neuregulin receptor ErbB4. *Nat. Cell Biol.* **2**, 103-109.
Goronowitsch, N. (1893). Untersuchungen uber die Entwickelung der sog. 'Ganglionleisten' im Kopfe der Vogelembryonen. *Morphologisches Jahrbuch* **20**, 187-260.
Graham, A., Blentic, A., Duque, S. and Begbie, J. (2007). Delamination of cells from neurogenic placodes does not involve an epithelial-to-mesenchymal transition. *Development* **134**, 4141-4145.
Hamburger, V. and Hamilton, H. L. (1992). A series of normal stages in the development of the chick embryo. 1951. *Dev. Dyn.* **195**, 231-272.
Harlow, D. E., Yang, H., Williams, T. and Barlow, L. A. (2011). Epibranchial placode-derived neurons produce BDNF required for early sensory neuron development. *Dev. Dyn.* **240**, 309-323.
Layer, P. G. and Kaulich, S. (1991). Cranial nerve growth in birds is preceded by cholinesterase expression during neural crest cell migration and the formation of an HNK-1 scaffold. *Cell Tissue Res.* **265**, 393-407.
Lois, C., García-Verdugo, J. M. and Alvarez-Buylla, A. (1996). Chain migration of neuronal precursors. *Science* **271**, 978-981.
López-Bendito, G., Cautinat, A., Sánchez, J. A., Bielle, F., Flames, N., Garratt, A. N., Talmage, D. A., Role, L. W., Charnay, P., Marín, O. et al. (2006). Tangential neuronal migration controls axon guidance: a role for neuregulin-1 in thalamocortical axon navigation. *Cell* **125**, 127-142.
McCabe, K. L., Sechrist, J. W. and Bronner-Fraser, M. (2009). Birth of ophthalmic trigeminal neurons initiates early in the placodal ectoderm. *J. Comp. Neurol.* **514**, 161-173.
Nguyen, Q. T., Sanes, J. R. and Lichtman, J. W. (2002). Pre-existing pathways promote precise projection patterns. *Nat. Neurosci.* **5**, 861-867.
Osborne, N. J., Begbie, J., Chilton, J. K., Schmidt, H. and Eickholt, B. J. (2005). Semaphorin/neuropilin signaling influences the positioning of migratory neural crest cells within the hindbrain region of the chick. *Dev. Dyn.* **232**, 939-949.
Parrinello, S., Napoli, I., Ribeiro, S., Wingfield Digby, P., Fedorova, M., Parkinson, D. B., Doddrell, R. D., Nakayama, M., Adams, R. H. and Lloyd, A. C. (2010). EphB signaling directs peripheral nerve regeneration through Sox2-dependent Schwann cell sorting. *Cell* **143**, 145-155.
Sauka-Spengler, T. and Bronner-Fraser, M. (2008). A gene regulatory network orchestrates neural crest formation. *Nat. Rev. Mol. Cell Biol.* **9**, 557-568.
Schwarz, Q., Vieira, J. M., Howard, B., Eickholt, B. J. and Ruhrberg, C. (2008). Neuropilin 1 and 2 control cranial gangliogenesis and axon guidance through neural crest cells. *Development* **135**, 1605-1613.
Sepp, K. J. and Auld, V. J. (2003). Reciprocal interactions between neurons and glia are required for Drosophila peripheral nervous system development. *J. Neurosci.* **23**, 8221-8230.
Sepp, K. J., Schulte, J. and Auld, V. J. (2001). Peripheral glia direct axon guidance across the CNS/PNS transition zone. *Dev. Biol.* **238**, 47-63.
Shiau, C. E. and Bronner-Fraser, M. (2009). N-cadherin acts in concert with Slit1-Robo2 signaling in regulating aggregation of placode-derived cranial sensory neurons. *Development* **136**, 4155-4164.
Shiau, C. E., Lwigale, P. Y., Das, R. M., Wilson, S. A. and Bronner-Fraser, M. (2008). Robo2-Slit1 dependent cell-cell interactions mediate assembly of the trigeminal ganglion. *Nat. Neurosci.* **11**, 269-276.
Shigetani, Y., Howard, S., Guidato, S., Furushima, K., Abe, T. and Itasaki, N. (2008). Wise promotes coalescence of cells of neural crest and placode origins in the trigeminal region during head development. *Dev. Biol.* **319**, 346-358.
Srinivas, S., Watanabe, T., Lin, C. S., William, C. M., Tanabe, Y., Jessell, T. M. and Costantini, F. (2001). Cre reporter strains produced by targeted insertion of EYFP and ECFP into the ROSA26 locus. *BMC Dev. Biol.* **1**, 4.
Thompson, H., Blentic, A., Watson, S., Begbie, J. and Graham, A. (2010). The formation of the superior and jugular ganglia: insights into the generation of sensory neurons by the neural crest. *Dev. Dyn.* **239**, 439-445.
Tucker, G. C., Aoyama, H., Lipinski, M., Tursz, T. and Thiery, J. P. (1984). Identical reactivity of monoclonal antibodies HNK-1 and NC-1: conservation in vertebrates on cells derived from the neural primordium and on some leukocytes. *Cell Differ.* **14**, 223-230.

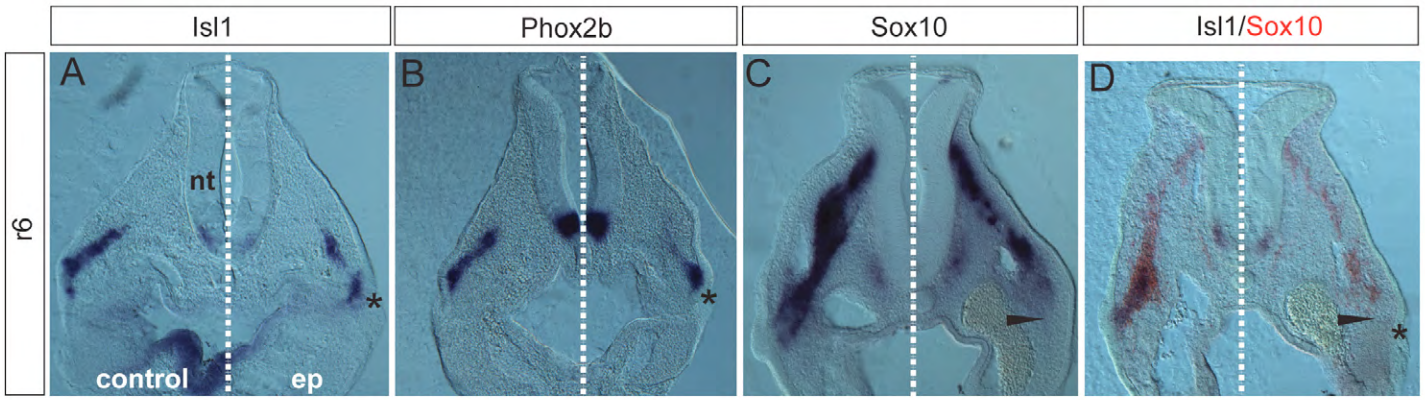

Fig. S1. Ablation of more posterior placode also affects neural crest corridor formation. (**A**,**B**) Sections at r6 level show that there is a reduction in neuroblasts seen with *Isl1* (A) and *Phox2b* (B) from the targeted petrosal placode (asterisks) on ep compared with control sides. (**C**,**D**) Staining for *Sox10* (C) shows an effect on NCC corridor extension (arrowhead) and double staining for *Isl1*/*Sox10* (D) confirms that the reduction in NCC corridor (arrowhead) correlates with loss of neuroblasts (asterisks). nt, neural tube; r, rhombomere; ep, electroporated.

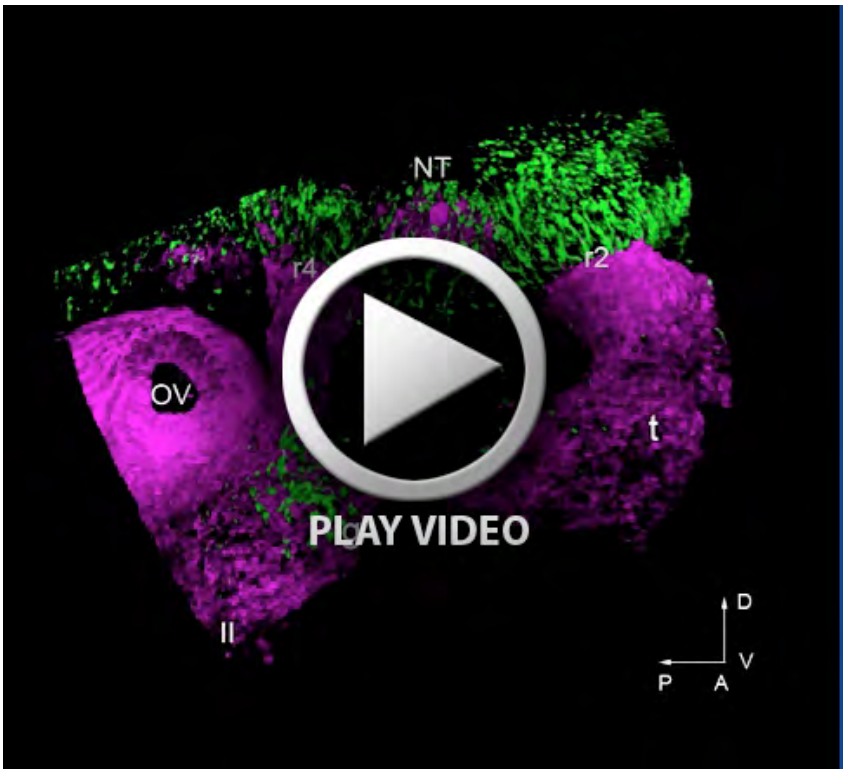

Movie 1. Neural crest cells form a robust structure extending between hindbrain and pharyngeal arches. Three-dimensional reconstruction of confocal *z*-stack through HH17 chicken embryo antibody labelled for HNK1 (neural crest, magenta) and NFM (neurons, green). Imaged region corresponds to R2 and R4 neural crest streams anterior to the otic vesicle. Initial orientation before rotation is equivalent to Fig 1A. NT, neural tube; OV, otic vesicle; r, rhombomere; t and g, developing trigeminal and geniculate ganglia; II, pharyngeal arch 2. Axes indicated: D, dorsal; V, ventral; A, anterior; P, posterior.

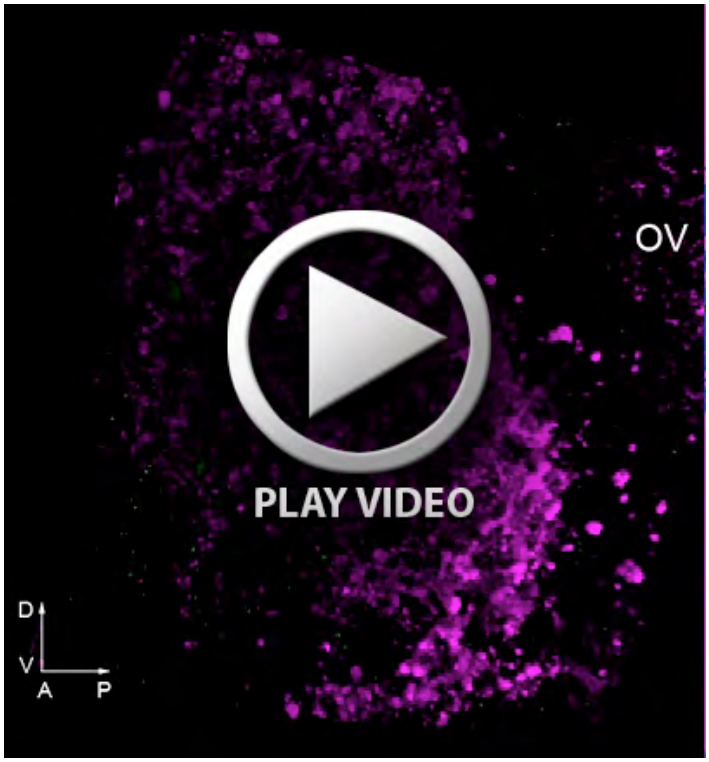

Movie 2. Neural crest cells form a corridor associated with neuroblast migration. Three-dimensional reconstruction of a confocal *z*-stack taken through a HH17 chicken embryo showing a GFP-labelled neuroblast migrating within the HNK1^{+} NCC corridor. The region imaged corresponds to the R2 neural crest stream. Initial view shows the exterior of the HNK1^{+} NCC corridor (magenta) then *z*-stack is rotated to show middle of NCC corridor revealing GFP^{+} neuroblast (green). Final rotation shows a coronal angle through the HNK1^{+} NCC corridor. OV, otic vesicle. Axes as before.

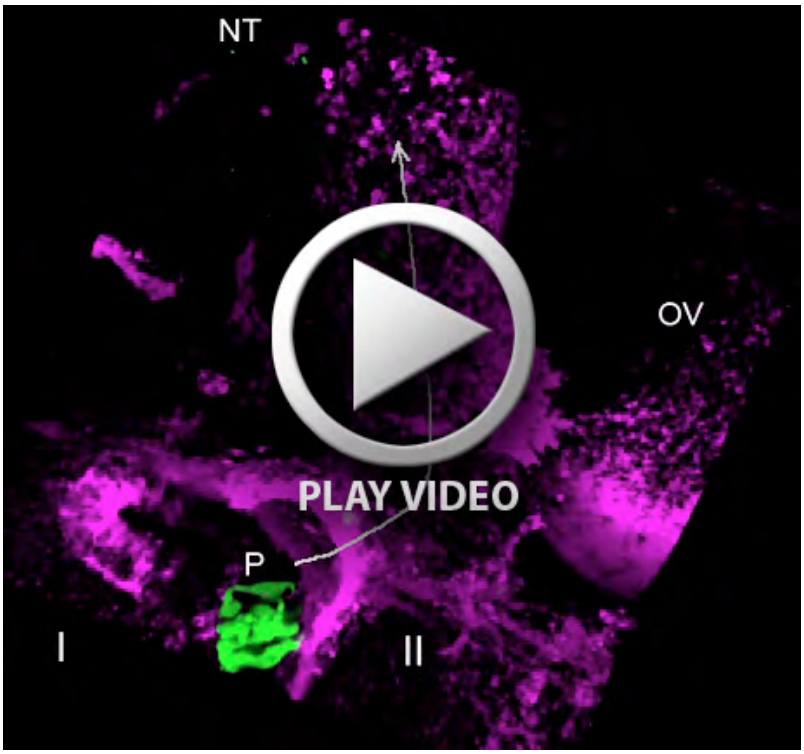

Movie 3. HNK1 NCC corridor extends to the placodal epithelium. Three-dimensional reconstruction of a confocal *z*-stack through HH17 chicken embryo showing HNK1^{+} NCC corridor extending to GFP-labelled placode. Imaged region corresponds to R2 neural crest stream. Initial view shows the exterior of HNK1^{+} NCC corridor (magenta) forming a funnel at the placode. Rotation reveals GFP neurons migrating within the NCC corridor. Following rotation back to the initial view, *Sox10 in situ* expression is added to show Sox10^{+} NCC within HNK1^{+} NCC corridor. I and II, pharyngeal arches 1 and 2; NT, location of neural tube; OV, otic vesicle; P, placode; arrow, direction of neuroblast migration.